IEICE TRANS. ELECTRON., VOL.E96–C, NO.10 OCTOBER 2013

PAPER Special Section on Emerging Technologies and Applications for Microwave and Millimeter-Wave Systems

Nonlinear Modeling and Analysis on Concurrent Amplification of Dual-Band Gaussian Signals

Ikuma ANDO[†a)], ***Nonmember***, **Gia Khanh TRAN**[†], ***Member***, **Kiyomichi ARAKI**[†], ***Fellow***, **Takayuki YAMADA**[††], ***Member***, **Takana KAHO**[††], **Yo YAMAGUCHI**[††], ***Senior Members***, ***and*** **Kazuhiro UEHARA**[††], ***Fellow***

SUMMARY In the recently developed Flexible Wireless System (FWS), the same platform needs to deal with different wireless systems. This increases nonlinear distortion in its wideband power amplifier (PA) because the PA needs to concurrently amplify multi-band signals. By taking higher harmonics as well as inter- and cross-modulation distortion into consideration, we have developed a method to analytically evaluate the adjacent channel leakage power ratio (ACPR) and error vector magnitude (EVM) on the basis of the PA's nonlinear characteristics. We devise a novel method for modeling the PA amplifying dual-band signals. The method makes it possible to model it merely by performing a one-tone test, making use of the Volterra series expansion and the general Wiener model. We then use the Mehler formula to derive the closed-form expressions of the PA's output power spectral density (PSD), ACPR, and EVM. The derivations are based on the assumption that the transmitted signals are complex Gaussian distributed in orthogonal frequency division multiplexing (OFDM) transmission systems. We validate the method by comparing measurement and simulation results and confirm it can appropriately predict the ACPR and EVM performance of the nonlinear PA output with OFDM inputs. In short, the method enables correct modeling of a wideband PA that amplifies dual-band signals merely by conducting a one-tone test.

key words: *nonlinear power amplifier, spectral regrowth, ACPR, EVM, OFDM, complex Gaussian distribution, Flexible Wireless System, Volterra series expansion, general Wiener model*

1. Introduction

A wide variety of wireless systems has been developed for providing ubiquitous network services. However, the increasing number of such systems causes problems such as lack of space for deploying base stations and interference from wireless terminals of different systems. A solution to these problems has been developed in the form of a common platform dealing with different wireless systems, i.e., the "Flexible Wireless System" (FWS) [1]. In FWS, an access point needs to concurrently handle multi-band signals of various wireless systems such as WiFi, cellular, and radio frequency identification (RFID) systems. Transmitters in conventional wireless systems only transmit signals of a specific system at one frequency band. In conventional transmitters, the number of RF circuits would increase proportionally to the number of wireless systems and frequency bands. As a first step to reducing the number of RF circuits, this paper examines a wideband power amplifier (PA) that amplifies multi-band signals concurrently.

Power amplifiers inherently have nonlinear characteristics for large input signals and generate spectral regrowth at the output. This spectral regrowth results in a large amount of interference on adjacent channels and decreases spectral efficiency. Using the output power back-off technique is a simple way to avoid this problem; it can be used to operate PAs in the linear region, and it decreases nonlinear distortion. However, this approach results in poor power efficiency because PAs only achieve high power efficiency around the saturation point [2]. Thus, there is a trade-off between linearity and power efficiency. In the FWS, the nonlinearity of its PA amplifying multi-band signals becomes an increasingly severe problem because of the generation of not only single-band inter-modulation but also cross-modulation and harmonic distortion. In [3]–[8], the nonlinear characteristics of PAs were modeled so as to take inter- and cross-modulation into consideration. However, these studies considered only two-tone carriers with near frequencies and did not consider harmonic effects. In contrast, this paper models the nonlinear characteristics of a wideband PA, where the two-tone carrier has a relatively large frequency separation, with the harmonic effect taken into account, and clarifies the PA's nonlinear distortion for this novel scenario.

In communication systems, both the adjacent channel power ratio (ACPR) and error vector magnitude (EVM) are important communication quality parameters. While EVM is used to evaluate the in-band distortion, ACPR is used to evaluate the out-band distortion of other channels. Both parameters are regulated according to specific system requirements. This paper analytically derives the relationship between these parameters and the wideband PA's nonlinear characteristics and uses them as metrics for validating the effectiveness of our method for modeling the wideband PA. The analytic study also facilitates evaluation of the PA's nonlinear distortion based on closed-form expression, and it can be usefully applied to PA design procedure to fulfill various system requirements.

Orthogonal frequency division multiplexing (OFDM) transmission is used in recent wireless systems owing to its high spectral efficiency and robustness against multipath fading [9]. In this paper, therefore we use OFDM signals as the input signals to the wideband PA. This choice also facilitates our analysis because the OFDM waveform can

Manuscript received February 14, 2013.
Manuscript revised June 6, 2013.

[†]The authors are with Tokyo Institute of Technology, Tokyo, 152-8552 Japan.
[††]The authors are with NTT Network Innovation Laboratories, NTT Corporation, Yokosuka-shi, 239-0847 Japan.
a) E-mail: ando@mobile.ee.titech.ac.jp

DOI: 10.1587/transele.E96.C.1254

be considered to follow approximately a Gaussian distribution. It also makes analyzing the power spectrum density (PSD), EVM, and ACPR as easy as has been done in studies on single-band systems, e.g., in [10]–[14] for ACPR analysis and [15], [16] for EVM analysis. On the other hand, although [17] measured the ACPR of a dual-band OFDM system, their study lacked theoretical support. In contrast to these studies, this paper analytically investigates the EVM and ACPR output performance of dual-band OFDM signals input to a multi-octave band PA and compares the theoretical results with our measurement results.

The rest of the paper is organized as follows. Section 2 details our method for modeling the nonlinear characteristics of a PA concurrently amplifying dual-band signals. In Sect. 3, we explain the characteristics of an OFDM signal and theoretically analyze the PA nonlinearity. We also derive the PA output auto-correlation function (ACF) and the closed-form expressions of ACPR and EVM. Section 4 describes our conducted measurements to validate the modeling method. Furthermore, the model is employed to evaluate the nonlinear effect on concurrent amplification of OFDM signals by both analytical and numerical approaches. Section 5 concludes the paper with a summary of key points.

2. Modeling a Wideband Power Amplifier

Reports have previously been published on methods for modeling a nonlinear PA amplifying a single-band signal [18], [19]. However, no methods have yet been reported for modeling such a PA concurrently amplifying multi-band signals. Accordingly, in this section we propose such a method that uses the Volterra series expansion and the general Wiener model.

2.1 Volterra Series Expansion

The Volterra series has become one of the most often used tools for modeling and characterizing nonlinear systems [20]. The Volterra series for nonlinear time-invariant systems is defined as,

$$y(t) = \sum_{n=1}^{\infty} \int \cdots \int h_n(\tau_1, \ldots, \tau_n) \prod_{i=1}^{n} x(t-\tau_i) d\tau_i, \qquad (1)$$

where the response $y(t)$ is a sum of multi-dimensional integrals, $h_n(\tau_1, \ldots, \tau_n)$ is the nth-order impulse response, and $x(t)$ is the input signals in time domain. We can also describe the Volterra series in the frequency domain as

$$Y(\omega) = \sum_{n=1}^{\infty} \int \cdots \int H_n(\omega_1, \ldots, \omega_n) \times \delta\left(\omega - \sum_{i=1}^{n} \omega_i\right) \prod_{i=1}^{n} X(\omega_i) d\omega_i, \qquad (2)$$

where $Y(\omega), X(\omega), H_n(\omega_1, \ldots, \omega_n)$ are respectively the output, input, and nth-order Volterra kernel in the frequency domain. We can model the PA output by using the above equations. In this paper, we consider a two-tone (ω_1, ω_2) dual-band signal $X(\omega) = X(\omega_1)\delta(\omega - \omega_1) + X(\omega_2)\delta(\omega - \omega_2)$ and define the input and output signals as

$$x(t) = A_{\text{in}}^{(1)} \cos(\omega_1 t + \theta_{\text{in}}^{(1)}) + A_{\text{in}}^{(2)} \cos(\omega_2 t + \theta_{\text{in}}^{(2)})$$

$$X(\omega_k) = \frac{1}{2} A_{\text{in}}^{(k)} e^{j\theta_{\text{in}}^{(k)}} \qquad (3)$$

$$Y(\omega_k) = \frac{1}{2} A_{\text{out}}^{(k)} e^{j\theta_{\text{out}}^{(k)}} \ (k = 1, 2), \qquad (4)$$

where $A_{\text{in}}^{(k)}, e^{j\theta_{\text{in}}^{(k)}}, A_{\text{out}}^{(k)}, e^{j\theta_{\text{out}}^{(k)}}$ respectively denote the amplitude and phase of the input and output signals for the kth band. Considering only up to the third order Volterra kernel, we can express the output signal observed at the corresponding tone as

$$\begin{aligned} Y(\omega_1) &= H_1(\omega_1)X(\omega_1) \\ &\quad +3H_3(\omega_1, \omega_1, -\omega_1)X(\omega_1)|X(\omega_1)|^2 \\ &\quad +6H_3(\omega_1, \omega_2, -\omega_2)X(\omega_1)|X(\omega_2)|^2 \\ &\quad +3H_3(\omega_2, -\omega_1, -\omega_1)X(\omega_2)X(\omega_1)^{*2} \\ \text{or} \quad A_{\text{out}}^{(1)} e^{j(\theta_{\text{out}}^{(1)} - \theta_{\text{in}}^{(1)})} &= A_{\text{in}}^{(1)} H_1(\omega_1) \\ &\quad +3/4 A_{\text{in}}^{(1)^3} H_3(\omega_1, \omega_1, -\omega_1) \\ &\quad +3/2 A_{\text{in}}^{(1)} A_{\text{in}}^{(2)^2} H_3(\omega_1, \omega_2, -\omega_2) \\ &\quad +3/4 A_{\text{in}}^{(1)^2} A_{\text{in}}^{(2)} e^{j(\theta_{\text{in}}^{(2)} - 3\theta_{\text{in}}^{(1)})} \\ &\quad \times H_3(\omega_2, -\omega_1, -\omega_1) \qquad (5) \\ Y(\omega_2) &= H_1(\omega_2)X(\omega_2) \\ &\quad +3H_3(\omega_2, \omega_2, -\omega_2)X(\omega_2)|X(\omega_2)|^2 \\ &\quad +6H_3(\omega_2, \omega_1, -\omega_1)X(\omega_2)|X(\omega_1)|^2 \\ &\quad +H_3(\omega_1, \omega_1, \omega_1)X(\omega_1)^3 \\ \text{or} \quad A_{\text{out}}^{(2)} e^{j(\theta_{\text{out}}^{(2)} - \theta_{\text{in}}^{(2)})} &= A_{\text{in}}^{(2)} H_1(\omega_2) \\ &\quad +3/4 A_{\text{in}}^{(2)^3} H_3(\omega_2, \omega_2, -\omega_2) \\ &\quad +3/2 A_{\text{in}}^{(1)^2} A_{\text{in}}^{(2)} H_3(\omega_2, \omega_1, -\omega_1) \\ &\quad +1/4 A_{\text{in}}^{(1)^3} e^{j(3\theta_{\text{in}}^{(1)} - \theta_{\text{in}}^{(2)})} \\ &\quad \times H_3(\omega_1, \omega_1, \omega_1). \qquad (6) \end{aligned}$$

In Eqs. (5) and (6), the first and second terms correspond to the output of each tone's input, the third term corresponds to both tone's inputs, and the fourth term expresses the special case where ω_2 is the 3rd-harmonic wave of ω_1 (i.e., $\omega_2 = 3\omega_1$). Although the Volterra kernels of the first and second terms can be easily estimated by a one-tone measurement, estimating those of the third and fourth terms is difficult. In the next section, we will explain our method for estimating these Volterra kernels.

2.2 General Wiener Model

The general Wiener model decomposes a nonlinear system into three parts. The first part is an input matching circuit with frequency characteristics, the second part has nonlinear characteristics, and the third part is an output matching

circuit, also with frequency characteristics [20]. The PA frequency response is accordingly expressed as

$$H_n(\omega_1, \ldots, \omega_n) = \prod_{i=1}^{n} F(\omega_i) K_n G\left(\sum_{i=1}^{n} \omega_i\right), \tag{7}$$

where $F(\omega)$ denotes the input matching circuit frequency response, the term K_n represents the nonlinear coefficients, and $G(\omega)$ is the output matching circuit frequency response. In this paper, we assume that the frequency characteristics of the input matching circuit can be neglected (i.e., $F(\omega_1) = F(\omega_2)$). Accordingly, we can transform the third term of Eq. (5) as follows:

$$\begin{aligned} H_3(\omega_1, \omega_2, -\omega_2) &= F(\omega_1)|F(\omega_2)|^2 K_3 G(\omega_1) \\ &\approx F(\omega_1)|F(\omega_1)|^2 K_3 G(\omega_1) \\ &= H_3(\omega_1, \omega_1, -\omega_1). \end{aligned} \tag{8}$$

Therefore, in the same way, we can model a nonlinear PA concurrently amplifying dual-band signals merely by performing a one-tone signal test.

3. Nonlinear Distortion Analysis of OFDM Signals

In this section, we show the theoretical analysis of the output characteristics of a PA concurrently amplifying two OFDM signals in separated frequency bands.

3.1 Characteristics of OFDM Signals

The configuration of an OFDM transmitter for dual-band signals is shown in Fig. 1. Digitally modulated data are transformed into a time series by an inverse fast Fourier transform (IFFT). Guard intervals (GI) are then inserted, and the time series is reshaped by a window function. Finally, the two OFDM signals are combined. Accordingly, the PA input signal $x(t)$ can be represented by

$$x(t) = x^{(1)}(t) + x^{(2)}(t), \tag{9}$$

where $x^{(1)}(t)$ is the OFDM signal of the lower carrier frequency ω_1 and $x^{(2)}(t)$ is that of the higher carrier frequency ω_2. According to the central limit theorem, a baseband OFDM signal that is the sum of multiple sub-carriers' signals can be assumed to have a complex Gaussian distribution [16]. Figure 2 compares the normalized probability density function (PDF) of the real part of an OFDM signal with a Gaussian distribution. Judging from the comparison, we can assume that an OFDM signal follows a Gaussian distribution. This paper uses this assumption to simplify the analysis.

3.2 Nonlinear PA Model

We used an equivalent envelope behavior model to demonstrate the output of the nonlinear PA in the time domain. To simplify the analysis, we consider only up to third-order PA nonlinearities.

$$\begin{aligned} y^{(1)}(t) &= a_1^{(1)} x^{(1)}(t) + a_3^{(1)} x^{(1)}(t)|x^{(1)}(t)|^2 \\ &\quad + b_3^{(1)} x^{(1)}(t)|x^{(2)}(t)|^2 + c_3^{(1)} x^{(1)}(t)^{*^2} x^{(2)}(t) \end{aligned} \tag{10}$$

$$\begin{aligned} y^{(2)}(t) &= a_1^{(2)} x^{(2)}(t) + a_3^{(2)} x^{(2)}(t)|x^{(2)}(t)|^2 \\ &\quad + b_3^{(2)} x^{(1)}(t)^3 + c_3^{(2)} x^{(2)}(t)|x^{(1)}(t)|^2, \end{aligned} \tag{11}$$

where $y^{(1)}(t)$ is the PA output signal of the lower carrier frequency ω_1 and $y^{(2)}(t)$ is that of the higher carrier frequency

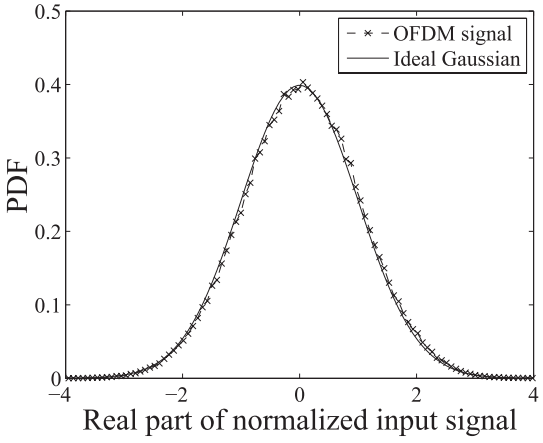

Fig. 2 PDF of real part of OFDM signals.

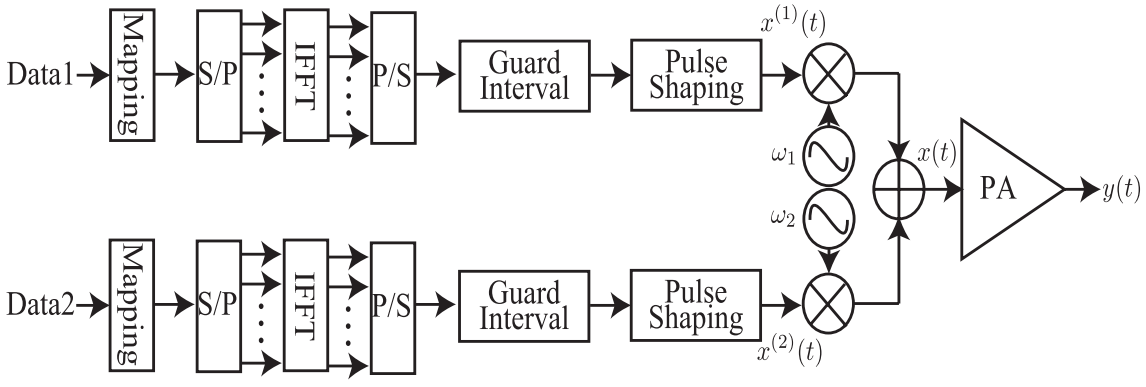

Fig. 1 OFDM transmitter for dual-band signals.

Table 1 Correspondence between the envelope coefficients and the Volterra kernels.

Coefficient	$k = 1$	$k = 2$
$a_1^{(k)}$	$H_1(\omega_1)$	$H_1(\omega_2)$
$a_3^{(k)}$	$3H_3(\omega_1, \omega_1, -\omega_1)/4$	$3H_3(\omega_2, \omega_2, -\omega_2)/4$
$b_3^{(k)}$	$3H_3(\omega_1, \omega_2, -\omega_2)/2$	$H_3(\omega_1, \omega_1, \omega_1)/4$
$c_3^{(k)}$	$3H_3(\omega_2, -\omega_1, -\omega_1)/4$	$3H_3(\omega_2, \omega_1, -\omega_1)/4$

ω_2. Table 1 shows the relation between the complex coefficients $a_1^{(k)}, a_3^{(k)}, b_3^{(k)}, c_3^{(k)}$ with the Volterra kernels.

3.3 ACF of PA Output

Since it can be assumed that an OFDM signal has a complex Gaussian distribution, the Mehler formula [21] can be used to derive the ACF of the normalized PA output. First, for each PA input signal $x^{(k)}(t)$ with zero mean and variance $2\sigma_k^2$, its normalized probability density function is expressed as

$$p(z^{(k)}) = \frac{1}{2\pi} e^{-\frac{|z^{(k)}|^2}{2}}, \tag{12}$$

where $z^{(k)}(t) = x^{(k)}(t)/\sigma_k$ $(k = 1, 2)$. Second, the joint probability density function of two random variables $z_1^{(k)} = z^{(k)}(t_1)$, $z_2^{(k)} = z^{(k)}(t_2) = z^{(k)}(t_1 + \tau)$ is

$$p(z_1^{(k)}, z_2^{(k)}) = \sum_{m,n=0}^{\infty} \Lambda_k^m \Lambda_k^{*n} \frac{F_{mn}(z_1^{(k)}) F_{nm}(z_2^{(k)})}{m! n! 2^{m+n}} \tag{13}$$

$$\Lambda_k(\tau) = \frac{\mathbb{E}[z_1^{(k)*} z_2^{(k)}]}{\sqrt{\mathbb{E}[z_1^{(k)*} z_1^{(k)}]\mathbb{E}[z_2^{(k)*} z_2^{(k)}]}} \approx \frac{R_{xx}^{(k)}(\tau)}{R_{xx}^{(k)}(0)}$$

$$F_{mn}(z^{(k)}) = p(z^{(k)}) H_{mn}(z^{(k)})$$

$$H_{mn}(z^{(k)}) = (-2)^{m+n} e^{z^{(k)} z^{(k)*}/2} \frac{\partial^n}{\partial z^{(k)n}} \frac{\partial^m}{\partial z^{(k)*m}} e^{-z^{(k)} z^{(k)*}/2}$$

$$R_{xx}^{(k)}(\tau) = \frac{1}{T_s'} \int_{-T_s'/2}^{T_s'/2} \mathbb{E}[x^{(k)*}(t_1) x^{(k)}(t_2)] dt_1$$

$$T_s' = T_s + T_g,$$

where Λ_k represents the ACF of the PA input signal, $\mathbb{E}[\cdot]$ represents the expectation operator, $H_{mn}(z)$ is a complex Hermite polynomial, T_s the IFFT length, T_g the GI length, and T_s' the OFDM symbol length. Third, the ACF of the PA output signal $y(t) = y^{(1)}(t) + y^{(2)}(t)$ can be derived as follows:

$$\begin{aligned}
\mathbb{E}[y^*(t) y(t+\tau)] &= \mathbb{E}[(y^{(1)^*}(t) + y^{(2)^*}(t)) \\
&\quad \times (y^{(1)}(t+\tau) + y^{(2)}(t+\tau))] \\
&= \mathbb{E}[y^{(1)^*}(t) y^{(1)}(t+\tau)] \\
&\quad + \mathbb{E}[y^{(2)^*}(t) y^{(2)}(t+\tau)] \\
&= \Phi_1^{\text{out}}(\tau) + \Phi_2^{\text{out}}(\tau),
\end{aligned} \tag{14}$$

where Φ_k^{out} is defined as $\mathbb{E}[y^{(k)^*}(t) y^{(k)}(t+\tau)]$. Note that $\mathbb{E}[y^{(1)^*}(t) y^{(2)}(t+\tau)] = \mathbb{E}[y^{(2)^*}(t) y^{(1)}(t+\tau)] = 0$, as there is no correlation between $x^{(1)}(t)$ and $x^{(2)}(t)$. Finally, from Eqs. (10), (11) and (13), the ACF of the output signal at each tone can be derived as

$$\begin{aligned}
\Phi_1^{\text{out}} &= \int\int\int\int y_1^{(1)^*} y_2^{(1)} p(z_1^{(1)}, z_2^{(1)}) \\
&\quad p(z_1^{(2)}, z_2^{(2)}) dz_1^{(1)} dz_2^{(1)} dz_1^{(2)} dz_2^{(2)} \\
&= (2|a_1^{(1)}|^2 \sigma_1^2 + 4 a_1^{(1)^*} b_3^{(1)} \sigma_1^2 \sigma_2^2 + 8 a_3^{(1)^*} a_1^{(1)} \sigma_1^4 \\
&\quad + 32|a_3^{(1)}|^2 \sigma_1^6 + 16 a_3^{(1)^*} b_3^{(1)} \sigma_1^4 \sigma_2^2 \\
&\quad + 4 a_1^{(1)} b_3^{(1)^*} \sigma_1^2 \sigma_2^2 + 8|b_3^{(1)}|^2 \sigma_1^2 \sigma_2^4 \\
&\quad + 16 b_3^{(1)^*} a_3^{(1)} \sigma_1^4 \sigma_2^2 + 8 a_3^{(1)} a_1^{(1)^*} \sigma_1^4) \Lambda_1 \\
&\quad + 16|a_3^{(1)}|^2 \sigma_1^6 \Lambda_1 |\Lambda_1|^2 + 18|b_3^{(1)}|^2 \sigma_1^2 \sigma_2^4 \Lambda_1 |\Lambda_2|^2 \\
&\quad + 16|c_3^{(1)}|^2 \sigma_1^4 \sigma_2^2 \Lambda_1^{*2} \Lambda_2
\end{aligned} \tag{15}$$

$$\begin{aligned}
\Phi_2^{\text{out}} &= \int\int\int\int y_1^{(2)^*} y_2^{(2)} p(z_1^{(1)}, z_2^{(1)}) \\
&\quad p(z_1^{(2)}, z_2^{(2)}) dz_1^{(1)} dz_2^{(1)} dz_1^{(2)} dz_2^{(2)} \\
&= (2|a_1^{(2)}|^2 \sigma_2^2 + 8 a_3^{(2)^*} a_1^{(2)} \sigma_2^4 + 4 a_1^{(2)^*} c_3^{(2)} \sigma_1^2 \sigma_2^2 \\
&\quad + 8 a_1^{(2)^*} a_3^{(2)} \sigma_2^4 + 32|a_3^{(2)}|^2 \sigma_2^6 \\
&\quad + 16 a_3^{(2)^*} c_3^{(2)} \sigma_1^2 \sigma_2^4 + 4 a_1^{(2)} c_3^{(2)^*} \sigma_1^2 \sigma_2^2 \\
&\quad + 8|c_3^{(2)}|^2 \sigma_1^4 \sigma_2^2 + 16 c_3^{(2)^*} a_3^{(2)} \sigma_1^2 \sigma_2^4) \Lambda_2 \\
&\quad + 16|a_3^{(2)}|^2 \sigma_2^6 \Lambda_2 |\Lambda_2|^2 + 48|b_3^{(2)}|^2 \sigma_1^6 \Lambda_1^3 \\
&\quad + 18|c_3^{(2)}|^2 \sigma_1^4 \sigma_2^2 |\Lambda_1|^2 \Lambda_2,
\end{aligned} \tag{16}$$

where $y_1^{(k)} = y^{(k)}(t_1)$, $y_2^{(k)} = y^{(k)}(t_1 + \tau)$ for brevity. Thus, the output ACF of the PA can be represented by parameter coefficients modeling the PA, input ACF, and average power of the PA input signal. Detailed derivations are shown in the Appendix.

3.4 ACPR and EVM for PA

EVM is defined as the average magnitude of error between the nonlinear PA output and the ideal PA output. First, we define the ideal PA output signal $\tilde{y}^{(k)}(t)$ and the error signal $\Delta y^{(k)}(t)$ as

$$\tilde{y}^{(k)}(t) = a_1^{(k)} x^{(k)}(t), \quad \Delta y^{(k)}(t) = y^{(k)}(t) - \tilde{y}^{(k)}(t). \tag{17}$$

To calculate the average signal power, we substitute $\Lambda_1 = \Lambda_2 = 1$ at $\tau = 0$ in Eqs. (15) and (16). Thus EVM can be derived as follows:

$$\text{EVM}_1 = \sqrt{\frac{\mathbb{E}[|\Delta y^{(1)}(t)|^2]}{\mathbb{E}[|\tilde{y}^{(1)}(t)|^2]}} = \sqrt{\frac{\Phi_1^{\text{out}}(0)\Big|_{a_1^{(1)}=0}}{|a_1^{(1)}|^2 2\sigma_1^2}} \tag{18}$$

$$\begin{aligned}
\Phi_1^{\text{out}}(0)\Big|_{a_1^{(1)}=0} &= 48|a_3^{(1)}|^2 \sigma_1^6 + 26|b_3^{(1)}|^2 \sigma_1^2 \sigma_2^4 \\
&\quad + 16|c_3^{(1)}|^2 \sigma_1^4 \sigma_2^2 + 16 b_3^{(1)} a_3^{(1)^*} \sigma_1^4 \sigma_2^2 \\
&\quad + 16 b_3^{(1)^*} a_3^{(1)} \sigma_1^4 \sigma_2^2
\end{aligned}$$

$$\text{EVM}_2 = \sqrt{\frac{\mathbb{E}[|\Delta y^{(2)}(t)|^2]}{\mathbb{E}[|\tilde{y}^{(2)}(t)|^2]}} = \sqrt{\frac{\Phi_2^{\text{out}}(0)\Big|_{a_1^{(2)}=0}}{|a_1^{(2)}|^2 2\sigma_2^2}} \tag{19}$$

$$\Phi_2^{\text{out}}(0)\Big|_{a_1^{(2)}=0} = 48|a_3^{(2)}|^2\sigma_2^6 + 48|b_3^{(2)}|^2\sigma_1^6 + 26|c_3^{(2)}|^2\sigma_1^4\sigma_2^2 + 16a_3^{(2)}c_3^{(2)*}\sigma_1^2\sigma_2^4 + 16a_3^{(2)*}c_3^{(2)}\sigma_1^2\sigma_2^4.$$

Moreover, from the Wiener-Khintchine theorem, each value of the PA output power spectral density (PSD) can be derived on the basis of Eqs. (15) and (16) as

$$S_k(f) = \int_{-\infty}^{\infty} \Phi_k^{\text{out}}(\tau)e^{-j2\pi f\tau}d\tau \ (k = 1, 2). \tag{20}$$

ACPR is defined as the ratio between adjacent channel leakage power and main channel power. It can be derived from Eq. (20), as

$$\text{ACPR}_k = \frac{\int_{B_{\text{adj}}} S_k(f)df}{\int_{B_{\text{in}}} S_k(f)df}, \tag{21}$$

where B_{in} is the frequency band of the main channel and B_{adj} is that of the adjacent channel. From the above discussion, the EVM value can be calculated using the closed-form expressions in Eqs. (18) and (19). Note that Eqs. (18) and (19) depend on the input's average power and the parameter coefficients modeling the PA. Since these parameters can be estimated by merely performing a one-tone test as noted in Sect. 2, it can be concluded that EVM can also be predicted from one-tone test results alone. In the same way, the ACPR value can be calculated using the closed-form expression in Eq. (21).

4. Measurement of a Wideband Amplifier and Nonlinear Evaluation

In this section, we validate our method by comparing modeling and measurement results. Using the validated model, we then perform a theoretical analysis and simulation that show the nonlinear effect on concurrent amplification of OFDM signals.

4.1 Measurement Setup

We measured the nonlinear characteristics of a wideband amplifier. Two cases (one- and two-tone signal input) were tested. In the latter, we considered two combinations of tones, i.e., a 250 MHz continuous wave (CW) signal with a 650 MHz CW signal (non-harmonic case) and a 250 MHz CW signal with a 750 MHz CW signal (harmonic case). The experimental setup and conditions are shown in Fig. 3 and Table 2.

As an immediate measure to examine the validity of the modeling method, our experiment employed a commercial wideband amplifier presented in [22]. The linear gain of this amplifier is 28 dB, the operation bandwidth is 50 kHz to 10 GHz and, the 1 dB compression point is around −20 dBm. The CW input signals were generated from signal generators (SG1 and SG2 in Fig. 3). In each of the one-tone measurements, only one signal was generated from SG1 or SG2 and the input power was changed in 0.5 dB steps. We input the signal to the wideband amplifier and measured the output power by using a vector signal analyzer. In the two-tone measurements, two-tone signals were concurrently generated at the same level from both SG1 and SG2 and their input levels were also concurrently changed in 0.5 dB steps. The signals were then added together and input to the wideband amplifier. In the same way as for the one-tone measurements, we used the vector signal analyzer to measure the output power at each tone.

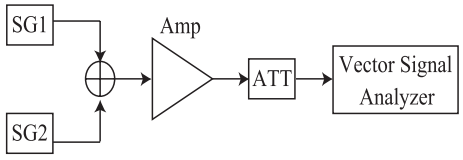

Fig. 3 Experimental setup.

Table 2 Experimental conditions.

SG1	Frequency: 250 MHz Transmitted power: −30 to −10 dBm
SG2	Frequency: 750/650 MHz Transmitted power: −30 to −10 dBm
ATT	18 dB
Vector Signal Analyzer	Span: 1 MHz IF BW: 50 kHz

Table 3 Estimated Volterra kernels from the one-tone measurement.

	250 MHz	650 MHz	750 MHz
$H(\omega)$	$24.5e^{-j1.206}$	$24.5e^{j1.4114}$	$24e^{-j1.204}$
$H(\omega,\omega,-\omega)$	$267.9e^{-j1.05}$	$335.9e^{-j1.26}$	$232.7e^{-j0.88}$
$H(\omega,\omega,\omega)$	$353.5e^{j0.368}$	-	-

4.2 Modeling Results

We first estimate the Volterra kernels in Eqs. (5) and (6) from the one-tone measurements of the wideband amplifier. Table 3 shows the estimated Volterra kernels derived by the one-tone test. We can further approximate other Volterra kernels modeling two-tone inputs from the estimated Volterra kernels by using the general Wiener model. Figure 4 shows the AM/AM characteristics for concurrent amplification of two-tone signals; it compares the modeling and measurement results we obtained. The figure indicates we can model the nonlinear amplifier characteristics for concurrent amplification of multi-tone signals by using Volterra series expansion and the general Wiener model where the wideband amplifier input power is between −30 dBm and −20 dBm. Here, the modeling results differ from the measured results where the amplifier input power is more than −20 dBm. This is because the paper mainly focuses on modeling the linear region. This region is suitable for designing a predistorter compensating for distortion because −20 dBm is the 1 dB compression point of the considered wideband amplifier. In Fig. 4(a), the output power of the 750 MHz

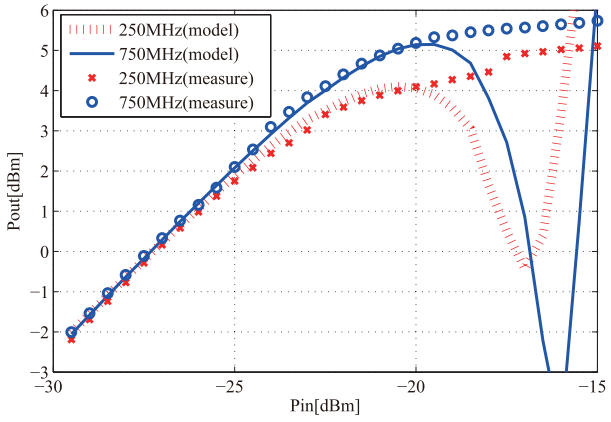

(a) 250 MHz and 750 MHz signals are concurrently input.

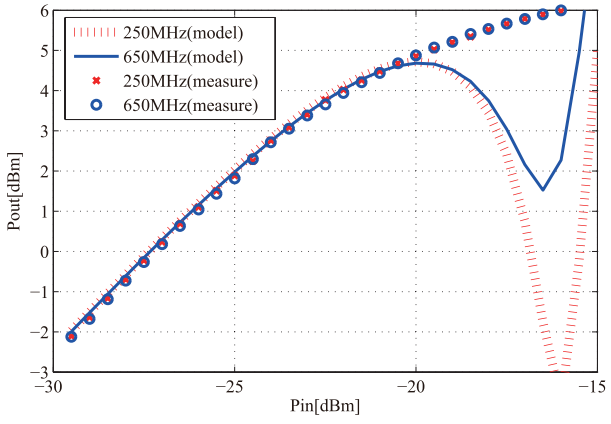

(b) 250 MHz and 650 MHz signals are concurrently input.

Fig. 4 Modeling on concurrent amplification of two-tone signals.

signal is higher than that of the 250 MHz signal when the two CW signals are concurrently input. The reason for the difference is that the value of the fourth term in Eq. (5) is different from that in Eq. (6) and both terms depend on the relative phase between the two input signals. On the other hand, in Fig. 4(b), the output power of the 650 MHz signal is the same as that of the 250 MHz signal when the two CW signals are concurrently input. The reason is that the fourth term in Eqs. (5) and (6) is not present in the case of a non-harmonic combination of tones while the Volterra kernels of the first to third terms have almost the same corresponding level.

4.3 Simulation Results

Table 4 lists the simulation parameters, which we obtained by referring to the IEEE 802.11a WLAN standard [23]. According to the standard, ACPR is defined as the ratio between the maximum output PSD and the output PSD at 20 MHz offset frequency where a 100 kHz resolution bandwidth is used to calculate the power.

Figure 5 shows the evaluation of the wideband amplifier input and output PSDs. The average input powers were set to −20 dBm, −25 dBm, and −30 dBm. All the PSDs are normalized by the in-band power of the input signal. The

Table 4 Simulation parameters.

Modulation	OFDM
Modulation in subcarriers	QPSK
Center frequencies	250 MHz, 750 MHz
Number of subcarriers	52
Number of FFT points	64
OFDM symbol duration	4.0 μs
Guard interval	0.8 μs
Bandwidth	20 MHz
$B_{\text{in}}, B_{\text{adj}}$	100 kHz
Roll-off factor β	0.025

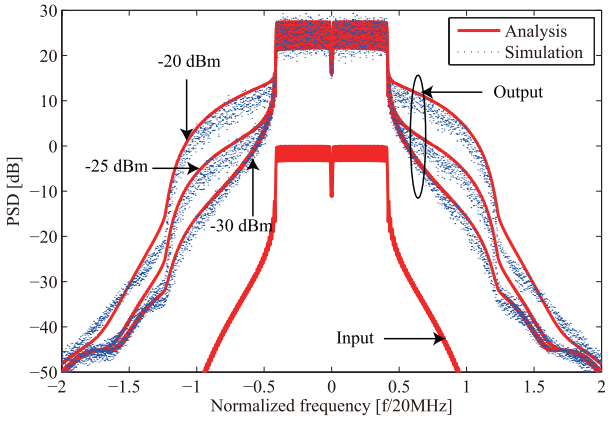

(a) 250 MHz.

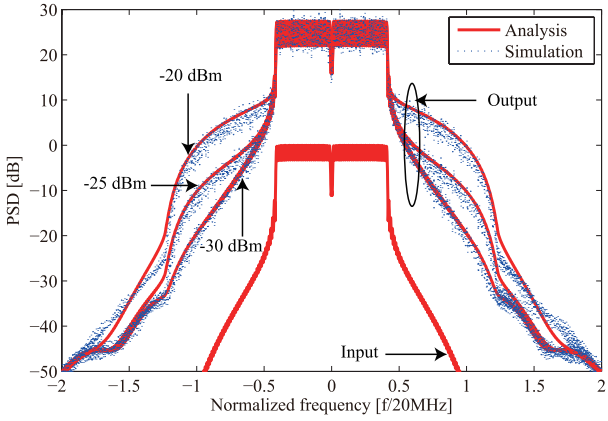

(b) 750 MHz.

Fig. 5 Spectral characteristics.

figure shows that the analytic results derived from Eq. (20) agree with the simulation results. Figure 6 compares the estimated EVM in Eqs. (18) and (19) and the estimated ACPR in Eq. (21) with those obtained in the simulation results. The horizontal axis is the back-off level; it is 0 dB at the 1 dB compression point of the wideband amplifier. The 1 dB compression point measured by the one-tone signal test is −20 dBm. We can see that the theoretical ACPR and EVM are coincident with the simulated results. When the back-off level is −5 dB, the EVMs of the 250 MHz and 750 MHz dual-band signals are respectively 6 dB and 2.5 dB higher than that of the one-tone signals. Similarly, the ACPR of the 250 MHz and 750 MHz dual-band signals is respectively

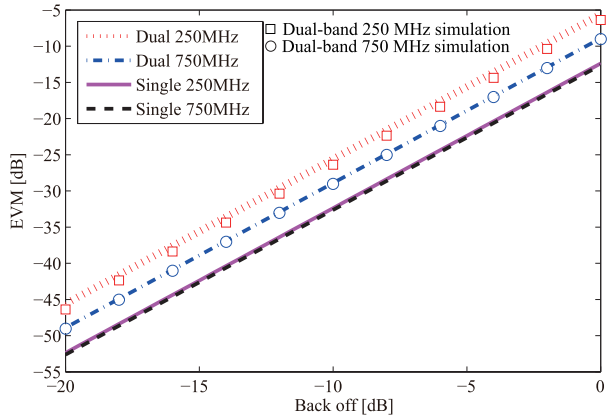

(a) EVM.

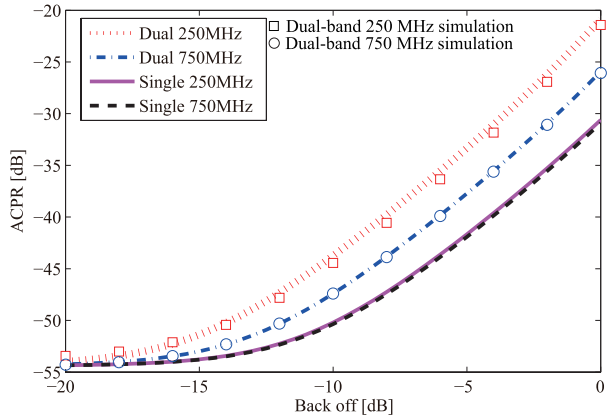

(b) ACPR.

Fig. 6 Theoretically analyzed and simulated results of EVM or ACPR vs. back off on concurrent input of 250 MHz and 750 MHz OFDM signals.

8 dB and 5 dB higher than that of the one-tone signals. As described above, these results show the EVM and ACPR increase when the dual-band signals are concurrently amplified because of cross-modulation, inter-modulation, and harmonic distortion. In conclusion, both the theoretical analysis and the simulation, which apply the model derived by a one-tone test, can show the effect of the wideband amplifier nonlinear characteristics on the concurrent amplification of two OFDM signals in dual bands.

5. Conclusion

In this paper, we used measured results to model the characteristics of a wideband amplifier concurrently amplifying two-tone continuous wave (CW) signals with largely separated frequencies, and showed the effective input power range for amplifiers. We also theoretically analyzed the nonlinear characteristics of a wideband amplifier concurrently driven with two orthogonal frequency division multiplexing (OFDM) signals by using the Mehler formula, since an OFDM signal envelope can be assumed to follow a Gaussian distribution. As a result of modeling the wideband amplifier and theoretically analyzing OFDM signals, we found that the nonlinear characteristics of a wideband amplifier concurrently amplifying dual OFDM signals can be revealed by performing a one-tone signal test.

References

[1] H. Shiba, Y. Yamaguchi, K. Akabane, T. Yamada, and K. Uehara, "A flexible wireless system supporting for a wide variety of wireless systems," IEICE Technical Report, SR2010-37, July 2010.
[2] F.H. Raab, P. Asbeck, S. Cripps, P.B. Kenington, Z.B. Popovic, N. Pothecary, J.F. Sevic, and N.O. Sokal, "Power amplifiers and transmitters for RF and microwave," IEEE Trans. Microw. Theory Tech., vol.50, pp.814–826, March 2002.
[3] W. Chen, S.A. Bassam, X. Lee, Y. Liu, K. Rawat, M. Helaoui, F.M. Ghannouchi, and Z. Feng, "Design and linearization of concurrent dual-band doherty power amplifier with frequency-dependent power ranges," IEEE Trans. Microw. Theory Tech., vol.59, no.10, pp.2537–2546, Oct. 2011.
[4] S.A. Bassam, M. Helaoui, and F.M. Ghannouchi, "2-D digital predistortion (2-D-DPD) architecture for concurrent dual-band transmitters," IEEE Trans. Microw. Theory Tech., vol.59, no.10, pp.2547–2553, Oct. 2011.
[5] S.A. Bassam, A. Kwan, W. Chen, M. Helaoui, and F.M. Ghannouchi, "Subsampling feedback loop applicable to concurrent dual-band linearization architecture" IEEE Trans. Microw. Theory Tech., vol.60, no.6, pp.1990–1999, June 2012.
[6] L. Ding, Z. Yang, and H. Gandhi, "Concurrent dual-band digital predistortion," Proc. IEEE MTT-S Int. Microwave Symposium Digest, June 2012.
[7] J. Kim, P. Roblin, X. Yang, and D. Chaillot, "A new architecture for frequency-selective digital predistortion linearization for RF power amplifiers," Proc. IEEE MTT-S Int. Microwave Symposium Digest, June 2012.
[8] H. Harada, H.J. Lee, S. Komaki, and N. Morinaga, "Performance analysis of fiber-optic millimeter-wave band radio subscriber loop," IEICE Trans. Commun., vol.E76-B, no.9, pp.1128–1135, Sept. 1993.
[9] L.J. Cimini, "Analysis and simulation of a digital mobile channel using orthogonal frequency division multiplexing," IEEE Trans. Commun, vol.33, pp.665–675, July 1985.
[10] Q. Wu, H. Xiao, and F. Li, "Linear RF power amplifier design for CDMA signals: A spectrum analysis approach," Microwave Journal, vol.41, no.12, pp.2240, Dec. 1998.
[11] K. Gard, H.M. Gutierrez, and M.B. Steer, "Characterization of spectral regrowth in microwave amplifiers based on the nonlinear transformation of a complex Gaussian process," IEEE Trans. Microw. Theory Tech., vol.47, no.7, pp.1059–1069, July 1999.
[12] K. Gard, M.B. Steer, and L.E. Larson, "Generalized autocorrelation analysis of spectral regrowth from bandpass nonlinear circuits," Proc. IEEE MTT-S Int. Microwave Symposium Digest, vol.1, pp.9–12, May 2001.
[13] G.T. Zhou and J.S. Kenney "Predicting spectral regrowth of nonlinear power amplifiers," IEEE Trans. Commun., vol.50, no.5, pp.718–722, May 2002.
[14] G.T. Zhou and R. Raich "Spectral analysis of polynomial nonlinearity with applications to RF power amplifiers," EURASIP J. Appl. Signal Process., vol.2004, no.12, pp.1831–1840, Sept. 2004.
[15] S. Yamanouchi, K. Kunihiro, and H. Hida, "OFDM error vector magnitude distortion analysis," IEICE Trans. Electron., vol.E89-C, no.12, pp.1836–1842, Dec. 2006.
[16] Y. Zhang and K. Araki, "A unified distortion analysis of nonlinear power amplifiers with memory effects for OFDM signals," IEICE Trans. Electron, vol.E93-C, no.4, pp.489–496, April 2010.
[17] P. Saad, P. Colantonio, J. Moon, L. Piazzon, F. Giannini, K. Andersson, B. Kim, and C. Fager, "Concurrent dual-band GaN-HEMT power amplifier at 1.8 GHz and 2.4 GHz," Wireless and Microwave Technology Conference (WAMICON), April 2012.

[18] A. Ahmed, M.O. Abdalla, E.S. Mengistu, and G. Kompa, "Power amplifier modeling using memory polynomial with non-uniform delay taps," 34-th European Microwave Conf. Proc., Amsterdam, Oct. 2004.
[19] H. Ku and J.S. Kenney, "Behavior modelling of nonlinear RF power amplifiers considering memory effects," IEEE Trans. Microw. Theory Tech., vol.51, no.12, pp.2495–2504, Dec. 2003.
[20] M. Schetzen, The Volterra and Wiener Theories of Nonlinear Systems (chapter 1), Revised ed., Kneiger Pub. Co, 2006.
[21] W.F. McGee, "Circularly complex Gaussian noise — A price theorem and a Mehler expansion," IEEE Trans. Inf. Theory, vol.IT-15, pp.317–319, March 1969.
[22] T. Yamada, I. Ando, G. Tran, K. Araki, T. Kaho, Y. Yamaguchi, K. Akabane, and K. Uehara, "A study on a digital predistortion for multi-band multi-signal transmission of flexible wireless system," IEICE Technical Report, SR2012-4, July 2012.
[23] Wireless LAN MAC and PHY Specifications: High-Speed Physical Layer in the 5 GHz Band, IEEE Standard 802.11a, 1999.

Appendix: PA Output ACF Derivation

Let us denote $x_1^{(k)} = x^{(k)}(t_1)$, $x_2^{(k)} = x^{(k)}(t_1+\tau)$, $y_1^{(k)} = y^{(k)}(t_1)$, $y_2^{(k)} = y^{(k)}(t_1+\tau)$. The complex Hermite polynomial has the following property:

$$\int \frac{1}{2\pi} e^{-|z|^2/2} H_{mn}(z) H_{\mu\nu}(z) dz = m!n!2^{m+n}\delta_{m\nu}\delta_{n\mu}. \quad (\text{A}\cdot 1)$$

Some examples of complex Hermite polynomials (order ≤ 3) are listed in Table A·1.

By using the complex Mehler expansion, we can derive the expected value of $z_1^{(k)\mu} z_1^{(k)*\nu} z_2^{(k)\gamma} z_2^{(k)*\lambda}$ as follows:

$$\begin{aligned}
&\mathbb{E}[z_1^{(k)\mu} z_1^{(k)*\nu} z_2^{(k)\gamma} z_2^{(k)*\lambda}] \\
&= \int z_1^{(k)\mu} z_1^{(k)*\nu} z_2^{(k)\gamma} z_2^{(k)*\lambda} p_i(z_1^{(k)}, z_2^{(k)}) dz_1^{(k)} dz_2^{(k)} \\
&= \sum_{m,n} \Lambda_k^m \Lambda_k^{*n} G_{\mu\nu,mn} G_{\gamma\lambda,nm} \quad (\text{A}\cdot 2)
\end{aligned}$$

$$\begin{aligned}
G_{\mu\nu,mn} &= \int \frac{p(z) z^\mu z^{*\nu} H_{mn}(z)}{\sqrt{m!n!2^{m+n}}} dz \quad (\text{A}\cdot 3) \\
&= \begin{cases} \text{positive number } (\mu+m=\nu+n) \\ \qquad\qquad \&(\nu+\mu \geq m+n) \\ 0 \qquad\qquad \text{else} \end{cases} \\
&= G_{\nu\mu,nm}.
\end{aligned}$$

The values of $G_{\mu\nu,mn}$ used in this paper are shown in Table A·2.

Thus, the ACF of the PA output in Eqs. (10) and (11) can be calculated by substituting Eqs. (A·2) and (A·3) into $\mathbb{E}[y_1^{(k)*} y_2^{(k)}]$. For brevity, we only show an example in which the first term in $y_1^{(1)}$ is multiplied by the third term in $y_2^{(1)}$. This results in $\mathbb{E}[a_1^{(1)*} x_1^{(1)*} b_3^{(1)} x_2^{(1)}(t) |x_2^{(2)}(t)|^2]$ as follows:

$$\begin{aligned}
&\mathbb{E}[a_1^{(1)*} x_1^{(1)*} b_3^{(1)} x_2^{(1)}(t) |x_2^{(2)}|^2] \\
&= a_1^{(1)*} b_3^{(1)} \sigma_1^2 \sigma_2^2 \mathbb{E}[z_1^{(1)*} z_2^{(1)} |z_2^{(2)}|^2] \\
&= a_1^{(1)*} b_3^{(1)} \sigma_1^2 \sigma_2^2 \int\int z_1^{(1)*} z_2^{(1)} p(z_1^{(1)}, z_2^{(1)}) dz_1^{(1)} dz_2^{(1)} \\
&\qquad \int\int z_2^{(2)} z_2^{(2)*} p(z_1^{(2)}, z_2^{(2)}) dz_1^{(2)} dz_2^{(2)} \\
&= a_1^{(1)*} b_3^{(1)} \sigma_1^2 \sigma_2^2 \sum_{m,n} \Lambda_1^m \Lambda_1^{*n} G_{01,mn} G_{10,nm} \\
&\qquad \sum_{i,j} \Lambda_2^i \Lambda_2^{*j} G_{00,ij} G_{11,ji} \\
&= 4 a_1^{(1)*} b_3^{(1)} \sigma_1^2 \sigma_2^2 \Lambda_1. \quad (\text{A}\cdot 4)
\end{aligned}$$

In the same way, other terms can also be calculated. Thus, Eqs. (15) and (16) can be analytically derived.

Table A·1 Complex Hermite polynomials.

H_{00}	1
H_{10}	z
H_{20}	z^2
H_{11}	$\|z\|^2 - 2$
H_{30}	z^3
H_{21}	$z^2 z^* - 4z$

Table A·2 Constant coefficients G.

mn	00	01	02	11	03	12
$G_{00,mn}$	1	0	0	0	0	0
$G_{10,mn}$	0	$\sqrt{2}$	0	0	0	0
$G_{20,mn}$	0	0	$2\sqrt{2}$	0	0	0
$G_{11,mn}$	2	0	0	3	0	0
$G_{30,mn}$	0	0	0	0	$4\sqrt{3}$	0
$G_{21,mn}$	0	$4\sqrt{2}$	0	0	0	4

Ikuma Ando received the B.E. degree in electrical engineering from Tokyo Institute of Technology, Tokyo, Japan, in 2012. He is currently working toward the M.E. degree at Tokyo Institute of Technology. His research interests include linearization of power amplifiers in flexible wireless systems and multiuser MIMO.

Gia Khanh Tran was born in Hanoi, Vietnam, on February 18, 1982. He received the B.E., M.E. and D.E. degrees in electrical and electronic engineering from Tokyo Institute of Technology, Japan, in 2006, 2008 and 2010 respectively. He received IEEE VTS Japan 2006 Young Researcher's Encouragement Award from IEEE VTS Japan Chapter in 2006, the Best Paper Award in Software Radio from IEICE SR technical committee in 2009 and 2013 respectively, and the IEICE service Recognition Award in 2013. His research interests are MIMO transmission algorithms, multiuser MIMO, MIMO mesh network and wireless power transmission. He is a member of IEEE.

Kiyomichi Araki was born in 1949. He received the B.S. degree in electrical engineering from Saitama University, in 1971, and the M.S. and Ph.D. degrees in physical electronics both from Tokyo Institute of Technology in 1973 and 1978 respectively. From 1973 to 1975, and from 1978 to 1985, he was a Research Associate at Tokyo Institute of Technology. From 1985 to 1995, he was an Associate Professor at Saitama University. In 1979–1980 and 1993–1994 he was a visiting research scholar at University of Texas, Austin and University of Illinois, Urbana, respectively. Since 1995 he has been a Professor at Tokyo Institute of Technology. His research interests are in information security, coding theory, communication theory, ferrite devices, RF circuit theory, electromagnetic theory, and microwave circuits, etc. He is a member of IEEE and Information Processing Society of Japan and fellow of IEICE. He is currently serving as a chair of Japan Chapter of IEEE MTT-S and a chair of Japan National committee of APMC.

Takayuki Yamada received the B.E. degree in electronics from Doshisha University, Kyoto, Japan, in 2005 and the M.E. degree in communications and computer engineering from the Graduate School of Informatics, Kyoto University, Kyoto, Japan, in 2007. Since joining NTT Network Innovation Laboratories in 2007, he has been engaged in research and development of flexible wireless systems. He received the Best Paper Award from IEICE Communications Society in 2012 and the Young Researchers Award from IEICE in 2013. He is a member of IEEE.

Takana Kaho is a Senior Research Engineer at Wireless Systems Innovation Laboratory, NTT Network Innovation Laboratories. She received the B.S. and M.S. degrees in physics from Tokyo Metropolitan University, Japan, in 1994 and 1996 respectively. She received the Dr. Eng. degree in communication engineering from Tokyo Institute of Technology, Japan, in 2007. She joined the NTT Radio Communication Systems Laboratories, Yokosuka, Japan, in 1996 and since has been engaged in research and development on MMICs. Since 2009, she has been an Expert Committee Member on the Information and Communications Council of the Ministry of Internal Affairs and Communications, Japan. Since 2010, she has been a Visiting Associate Professor at Research Institute of Electrical Communication, Tohoku University, Sendai, Japan. She received the Japan Microwave Prize at the 1998 Asia Pacific Microwave Conference and the Young Researchers' Award in 2004 presented by IEICE. She has served as a treasurer of the Japan Chapter of IEEE MTT-S since 2011.

Yo Yamaguchi received the B.S. and M.S. degrees in chemistry from Osaka University, Osaka, Japan, in 1989, and 1991, respectively. He received the D.E. degree in communication engineering from Tokyo Institute of Technology, Tokyo, Japan in 2010. In 1991, he joined NTT Radio Communication Systems Laboratories, Yokosuka, Japan, where he was engaged in research and development on MMIC's. From 1999 to 2001, he was an Associate Manager at STE Telecommunication Engineering Co., Ltd., where he served as a Technical Consultant on wireless communications. Since 2001, he has been a Senior Research Engineer at NTT Network Innovation Laboratories, Yokosuka, Japan. He received the Best Paper Award from the Institute of Electronics, Information and Communication Engineers (IEICE) Communication Society in 2012. He served as a Technical Program Committee (TPC) Vice Chair of the Asia Pacific Microwave Conference (APMC) 2010 and a secretary of the Institute of Electrical and Electronics Engineers (IEEE) Microwave Theory and Techniques Society Japan Chapter (MTT-SJC) Education Committee from 2009 to 2010. He is currently serving as a TRC Vice Chair of the APMC 2014, a committee member of the IEICE Technical Group on Microwave Engineering and a secretary of the International Union of Radio Science Commission C (URSI-C) Japan national committee. Dr. Yamaguchi is a member of the IEEE.

Kazuhiro Uehara is a Senior Manager of the Wireless Systems Innovation Laboratory, NTT Network Innovation Laboratories. He received the B.E., M.E., and Ph.D. degrees from Tohoku University, Miyagi, in 1987, 1989, and 1992, respectively. In 1992, he joined NTT and engaged in research on array antennas, active antennas and indoor propagation in the millimeter-wave and microwave frequency bands. From 1997 to 1998, he was a Visiting Associate at the Department of Electrical Engineering, California Institute of Technology, USA. He was a part-time lecturer at the Department of Electrical Engineering, Tohoku University from 2003 to 2010, and at the School of High-Technology for Human Welfare, Tokai University from 2009 to 2011. His current interests include research and development of software defined radio and cognitive radio systems and millimeter-wave multi-gigabit wireless systems. From 2009 to 2011, he was Chair of the Technical Committee on Software Radio, TCSR, IEICE Communication Society. He was a General Co-Chair of the 6th International Conference on Cognitive Radio Oriented Wireless Networks and Communications, CrownCom, June 2011. He is a Guest Editor-in-Chief of the Special Section on Wireless Distributed Networks, and the Special Section on Cognitive Radio and Heterogeneous Wireless Networks in Conjunction with Main Topics of CrownCom2011, IEICE Transactions on Communications, December 2010 and April 2012, respectively. From 2011, he is an Adviser of the TCSR, and a Councilor of Tokyo Section, IEICE. He received the Young Researcher's Award, the Best Paper Award, the Communications Society Outstanding Contributions Award, and the Communications Society Distinguished Contributions Award from IEICE in 1995, 1997, and twice in 2011 and 2012, respectively, the 1st YRP Award, and the 18th Telecom System Technology Award from the Telecommunications Advancement Foundation in 2002 and 2003, respectively. He is a senior member of IEEE.